Journal of Sound and Vibration 329 (2010) 4313–4332

Contents lists available at ScienceDirect

Journal of Sound and Vibration

journal homepage: www.elsevier.com/locate/jsvi

Microelectromechanical bandpass filters based on cyclic coupling architectures

Venkata Bharadwaj Chivukula [a,b], Jeffrey F. Rhoads [a,b,c,*]

[a] School of Mechanical Engineering, Purdue University, 585 Purdue Mall, West Lafayette, IN 47907, USA
[b] Birck Nanotechnology Center, Purdue University, 1205 W. State Street, West Lafayette, IN 47907, USA
[c] Ray W. Herrick Laboratories, Purdue University, 140 S. Martin Jischke Drive, West Lafayette, IN 47907, USA

ARTICLE INFO

Article history:
Received 1 January 2010
Received in revised form
15 April 2010
Accepted 20 April 2010
Handling Editor: D.J. Wagg

ABSTRACT

Bandpass filters based on resonant microelectromechanical systems (MEMS) have the unique advantage of being able to leverage the benefits of classical mechanical filters, including their high quality factors of resonance, while simultaneously addressing the challenges associated with manufacturing cost and size, and enabling integrated fabrication with other on-chip components. While prior research has demonstrated the benefits of microelectromechanical filters composed of both isolated and coupled microresonators, the optimality of existing filter architectures, and their associated performance metrics, is yet to be fully determined. To this end, the current effort seeks to investigate the relative utility of micromechanical filter designs which exploit a nontraditional filter architecture founded upon cyclic, elastic coupling. Specifically, the work seeks to characterize the pertinent performance metrics and robustness characteristics associated with these systems, and to benchmark the acquired results against conventional, open-chain filter designs. The work ultimately demonstrates that MEMS filters based upon cyclic coupling architectures may be beneficially leveraged in certain filter implementations to improve overall system performance.

1. Introduction

The past two decades have seen an increasing drive towards the miniaturization of highly selective, radio-frequency (RF) and intermediate-frequency (IF) bandpass signal filters. Given the inherent integrability limitations of conventional mechanical filters, such as those based on quartz crystals and surface acoustic wave (SAW) devices, the signal processing and wireless communications communities' research focus has been largely directed towards the development of filters based on isolated or coupled, resonant microelectromechanical systems (MEMS). As noted in prior literature, these devices not only offer comparatively high quality factors and appreciable center/cut-off frequencies, but they can also provide improvements in cost, size, and other filter performance and power metrics (including shape factor and insertion loss), while simultaneously facilitating seamless integration with other on-chip components [1–10]. To date, the vast majority of research pertaining to filters based on coupled microresonators has focused on open-chain architectures, wherein the internal elements of the microresonator array are coupled to their two nearest neighbors, and the terminating (end) elements are coupled to a single neighbor and an input or output port, as shown schematically in Fig. 1. Prior research in this area is typified by the works of Nguyen [4], who examined a filter architecture based on two folded-beam, lateral

* Corresponding author at: School of Mechanical Engineering, Purdue University, 585 Purdue Mall, West Lafayette, IN 47907, USA.
E-mail addresses: vchivuku@purdue.edu (V. Bharadwaj Chivukula), jfrhoads@purdue.edu (J.F. Rhoads).

0022-460X/$ - see front matter © 2010 Elsevier Ltd. All rights reserved.
doi:10.1016/j.jsv.2010.04.022

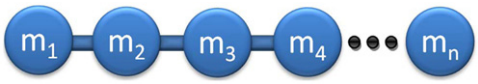

Fig. 1. Schematic of a filter based on n resonators coupled in an open-chain configuration.

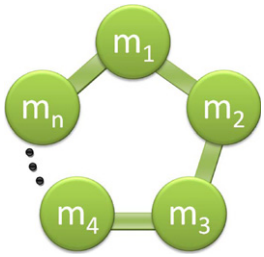

Fig. 2. Schematic of a filter based on n resonators coupled in a closed-chain configuration.

comb-driven resonators, and Bannon et al. [5], who considered two capacitively transduced, clamped–clamped beam resonators. Other efforts in this area have sought to leverage variations in resonator design [6,7], size, transduction [8–12], and number [13,14] to realize improved filter performance.

In 2002, Greywall and Busch introduced a new class of filters which challenged the optimality of existing designs [10]. These novel filters were founded upon a cyclically coupled (or closed-chain) architecture, in which all of the constituent microresonators were coupled to their two nearest neighbors, as shown in Fig. 2. The authors analyzed the response of both open- and closed-chain filters in their work, and demonstrated that in filter implementations in which the number of resonators in the coupled array was even, the closed-chain filter's frequency response exhibited a nominally symmetric passband with less ripple than its open-chain counterpart and reduced inter-band frequency dependence. The authors attempted to verify this results using electrostatically actuated, silicon nitride drumhead resonators, coupled through elastic overlap; however, the experimentally recovered frequency response for both of the utilized architectures showed appreciable ripple and a loss of the predicted degeneracy in the modal frequencies associated with each of the closed-chain filter designs. This was partially overcome by increasing the ambient pressure until there was sufficient overlap between the individual resonance peaks exhibited by the system, but the resulting low-ripple passband came at the expense of a reduced quality factor.

Though Greywall and Busch briefly highlighted the differences between the near-resonant response and associated metrics of filters based upon open- and closed-chain coupling architectures, their preliminary effort focused more on proof-of-concept development, than performance characterization and comparison [10]. In light of this, the current work seeks to build upon the earlier work of Greywall and Busch by developing a more comprehensive understanding of the relative utility of cyclically coupled resonator architectures in filter design. This is achieved by performing a thorough analysis of key filter metrics across the entirety of the feasible filter design space and by benchmarking the results acquired from closed-chain filters against those recovered from conventional, open-chain filter designs. In addition, a brief robustness analysis is performed to study the sensitivity of open- and closed-chain architectures to local variations in mass and stiffness, which are inevitably induced in the course of microfabrication. To this end, the paper is organized as follows. Section 2 details the mathematical modeling and analysis of open- and closed-chain filters. Section 3 summarizes numerical results recovered through simulation for open- and closed-chain filter designs which span a wide, yet realistic, range of coupling and dissipation, and details the results of a formal comparison between the various architectures' performance metrics. Section 4 considers the robustness of closed- and open-chain filters to process-induced variations, and the work ultimately concludes in Section 5 with a brief discussion and an overview of ongoing analytical and experimental efforts.

2. System modeling and analysis

To account for the breadth of resonator designs employed in MEMS filters (see, for example, [4–10]), a generic, lumped-parameter model, which is both transduction and geometry-independent is utilized for analysis. This model, shown schematically in Fig. 3, incorporates n lumped masses m_i, attached to massless linear springs of stiffness k_i and viscous dampers with damping coefficient c_i. Adjacent resonators are coupled by weak spring elements of stiffness k_c and viscous dampers with damping coefficient c_c. The equation of motion for the ith element of the system shown in Fig. 3 can be written as

$$m_i\ddot{y}_i + c_i\dot{y}_i + k_i y_i + c_c(-\dot{y}_{i-1} + 2\dot{y}_i - \dot{y}_{i+1}) + k_c(-y_{i-1} + 2y_i - y_{i+1}) = f_i(t), \quad (1)$$

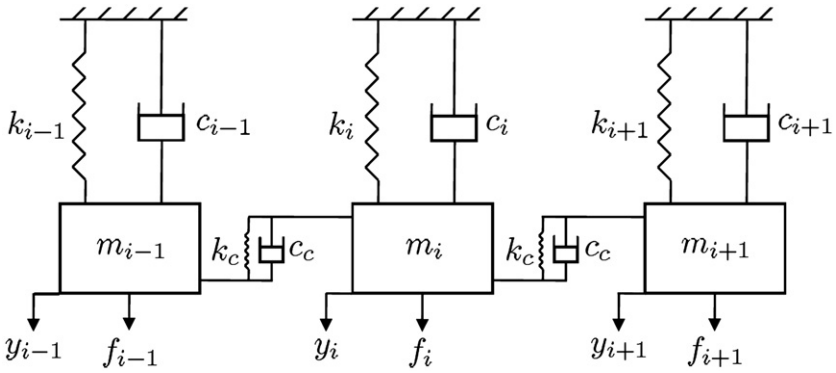

Fig. 3. Lumped-parameter model of an elastically coupled resonator chain.

where $f_i(t)$ represents an applied actuation force, which is assumed to be sinusoidal, provided by electrostatic, electromagnetic or piezoelectric means (Note, the results presented herein can be easily extended to account for multi-frequency inputs.). Nondimensionalizing this equation through the use of the nominal parameters given in Table 1 results in a final equation of motion for the system given in matrix form by

$$\mathbf{M}_{oc}\mathbf{Y}'' + \mathbf{C}_{oc}\mathbf{Y}' + \mathbf{K}_{oc}\mathbf{Y} = \mathbf{F}\cos(\Omega\tau), \tag{2}$$

where the mass, forcing, damping, and stiffness matrices are given, for a four-element, open-chain filter composed of identical elements, by

$$\mathbf{M}_{oc} = \begin{bmatrix} \hat{m}_1 & 0 & 0 & 0 \\ 0 & \hat{m}_2 & 0 & 0 \\ 0 & 0 & \hat{m}_3 & 0 \\ 0 & 0 & 0 & \hat{m}_4 \end{bmatrix}, \quad \mathbf{F} = \frac{1}{k_0 y_0}\begin{bmatrix} f_1 \\ f_2 \\ f_3 \\ f_4 \end{bmatrix},$$

$$\mathbf{C}_{oc} = \frac{1}{Q}\begin{bmatrix} \hat{c}_1+\hat{c}_c & -\hat{c}_c & 0 & 0 \\ -\hat{c}_c & \hat{c}_2+2\hat{c}_c & -\hat{c}_c & 0 \\ 0 & -\hat{c}_c & \hat{c}_3+2\hat{c}_c & -\hat{c}_c \\ 0 & 0 & -\hat{c}_c & \hat{c}_4+\hat{c}_c \end{bmatrix},$$

$$\mathbf{K}_{oc} = \begin{bmatrix} \hat{k}_1+\hat{k}_c & -\hat{k}_c & 0 & 0 \\ -\hat{k}_c & \hat{k}_2+2\hat{k}_c & -\hat{k}_c & 0 \\ 0 & -\hat{k}_c & \hat{k}_3+2\hat{k}_c & -\hat{k}_c \\ 0 & 0 & -\hat{k}_c & \hat{k}_4+\hat{k}_c \end{bmatrix}.$$

The response of this system can be recovered using classical impedance methods [15], which yield a solution of the form

$$\mathbf{Y}(i\Omega) = \mathbf{Z}_{oc}^{-1}(i\Omega)\mathbf{F}, \tag{3}$$

where

$$\mathbf{Z}_{oc}(i\Omega) = -\Omega^2\mathbf{M}_{oc} + i\Omega\mathbf{C}_{oc} + \mathbf{K}_{oc} \tag{4}$$

is the system's impedance matrix.

Fig. 4 shows the amplitude response of an open-chain system composed of six identical resonators with $\hat{c}_c = 0$, $\hat{k}_c = 0.02$, and Q=1000 when a unit amplitude force is applied solely to the first resonator in the chain (Given the linear nature of the system, alternative excitation amplitudes can be considered through the use of output scaling.). Analysis of this figure reveals that the resonator furthest from the drive (resonator 6) has the smallest amplitude outside the resonance region. This resonator is used to recover the filtered output. Note that a significant amplitude variation and asymmetry is observed inside of the resonance region due to the end resonators being coupled to only one resonator, while the interior constituents are coupled to their two nearest neighbors.

As noted above, in contrast to the open-chain architecture, closed-chain architectures have every element, including the first and the last, coupled to their two nearest neighbors, as shown schematically in Fig. 2. This results in modified stiffness and damping matrices which are symmetric and contain equal diagonal elements. For a 4-resonator, closed-chain filter,

Table 1
Parameter definitions.

Parameter	Description
$\omega_0 = \sqrt{\frac{k_0}{m_0}}$	Nominal natural frequency
$Q = \frac{m_0\omega_0}{c_0}$	Quality factor of isolated resonator
$\tau = \omega_0 t$	Nondimensional time
$\Omega = \frac{2\omega}{\omega_0}$	Nondimensional excitation frequency
$()' = \frac{\mathrm{d}()}{\mathrm{d}\tau}$	New derivative operator
$\hat{m}_i = \frac{m_i}{m_0}$	Nondimensional mass
$\hat{c}_i = \frac{c_i}{c_0}$	Nondimensional damping ratio
$\hat{c}_c = \frac{c_c}{c_0}$	Nondimensional dissipative coupling ratio
$\hat{k}_i = \frac{k_i}{k_0}$	Nondimensional stiffness ratio
$\hat{k}_c = \frac{k_c}{k_0}$	Nondimensional elastic coupling ratio
$\hat{y}_i = \frac{y_i}{y_0}$	Nondimensional displacement

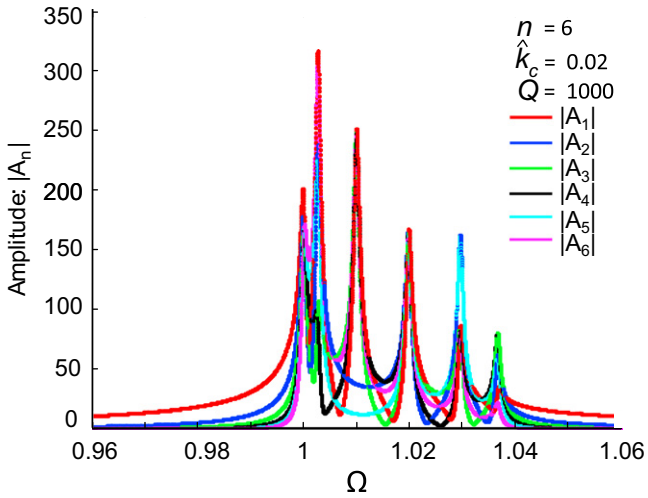

Fig. 4. Amplitude response of a 6-resonator, open-chain filter. Note that the actuation signal is applied only to resonator 1 and the output signal is measured at each of the respective resonators. Note that a well-formed passband does not exist for the selected set of parameters, this is to further exemplify key features of the system's frequency response, including its asymmetry.

these matrices become

$$\mathbf{C}_{cc} = \frac{1}{Q}\begin{bmatrix} \hat{c}_1+2\hat{c}_c & -\hat{c}_c & 0 & -\hat{c}_c \\ -\hat{c}_c & \hat{c}_2+2\hat{c}_c & -\hat{c}_c & 0 \\ 0 & -\hat{c}_c & \hat{c}_3+2\hat{c}_c & -\hat{c}_c \\ -\hat{c}_c & 0 & -\hat{c}_c & \hat{c}_4+2\hat{c}_c \end{bmatrix},$$

$$\mathbf{K}_{cc} = \begin{bmatrix} \hat{k}_1+2\hat{k}_c & -\hat{k}_c & 0 & -\hat{k}_c \\ -\hat{k}_c & \hat{k}_2+2\hat{k}_c & -\hat{k}_c & 0 \\ 0 & -\hat{k}_c & \hat{k}_3+2\hat{k}_c & -\hat{k}_c \\ -\hat{k}_c & 0 & -\hat{k}_c & \hat{k}_4+2\hat{k}_c \end{bmatrix}.$$

While the modifications delineated above appear superficial, they have dramatic consequences on the system's response. First, due to the symmetry of the impedance matrix $\mathbf{Z}(i\Omega)$, the pth undamped natural frequency Ω_p associated with the system can be recovered in a closed form [16]

$$\Omega_p = \sqrt{1+2\hat{k}_c(1-\cos\phi_p)}, \qquad \phi_p = \frac{2\pi(p-1)}{n}. \tag{5}$$

Of particular note here is the degeneracy in the natural frequencies caused by the cosine function in the expression above. This leads to the presence of only $n/2+1$ distinct natural frequencies when n is even and $(n+1)/2$ distinct natural frequencies when n is odd. This trend continues even for damped natural frequencies. Fig. 5 shows the amplitude response of a closed-chain system consisting of six identical resonators with $\hat{c}_c = 0$, $\hat{k}_c = 0.005$, and $Q=1000$, when unit amplitude forcing is applied to resonator 1. As evident, the response of each of the resonators is nominally symmetric about the center frequency and contains only four peaks (not six), due to the aforementioned degeneracy. Resonator 4, which features the largest amplitude within, and the smallest amplitude outside of the resonance region, is the most suitable selection as the output port for the filter.

Fig. 6 compares the response amplitude and transmissions of 6-resonator open- and closed-chain filters with $\hat{k}_c = 0.001$ and $Q=1000$, parameters which yield a well-defined passband. From this comparison, it is evident that the closed-chain filter has the highest response amplitude (highest transmisison/lowest insertion loss), high selectivity, and a nominally symmetric passband, and thus provides superior filter metrics.

2.1. Bandpass filter specifications

Fig. 7 shows the transmission of a real filter, normalized with respect to the maximum amplitude and expressed in decibel scale. Note that in this work, transmission is defined as

$$\text{Transmission (dB)} = 20\log_{10}\left(\frac{A}{A_{\max}}\right), \tag{6}$$

where A is the amplitude of the system's harmonic response and $A_{\max}$ is its maximum value within the filter passband. The *cut-off frequency* is defined at the half-power points or at 3 dB attenuation in the transmission amplitude—see ω_{c1} and ω_{c2} in Fig. 7. The difference between the two cut-off frequencies is defined as the *bandwidth*; this denotes the frequency span of the passband of the filter. The frequency at the center of the cut-off frequencies is defined as the *center frequency*. *Quality factor* is defined as the ratio of center frequency to the bandwidth (defined at 3 dB attenuation). To distinguish the quality factors of the open- and closed-chain filters from that of the individual resonators which compose the filter, the term *effective quality factor* (EQF) is used to refer to the quality factor of the composite system. Minimum insertion loss is the ratio of signal amplitude without the filter installed to the signal amplitude with the filter installed, assuming both unit amplitude input and a linear relation between the input and the output are utilized. Summarizing these definitions:

- Bandwidth $=\omega_{c2}-\omega_{c1}$,
- Center frequency $=(\omega_{c1}+\omega_{c2})/2$,
- EQF $=(\omega_{c2}+\omega_{c1})/2(\omega_{c2}-\omega_{c1})$,

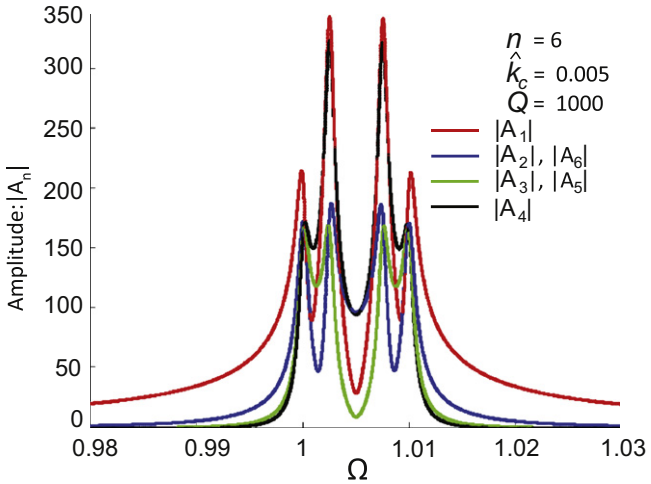

Fig. 5. Amplitude response at various resonators in a 6-resonator, closed-chain filter. Note that the excitation signal is applied to resonator 1 and the output is recovered at each of the respective resonators. Note that a well-formed passband does not exist for the selected set of parameters, this is to further exemplify key features of the system's frequency response, including its nominal symmetry.

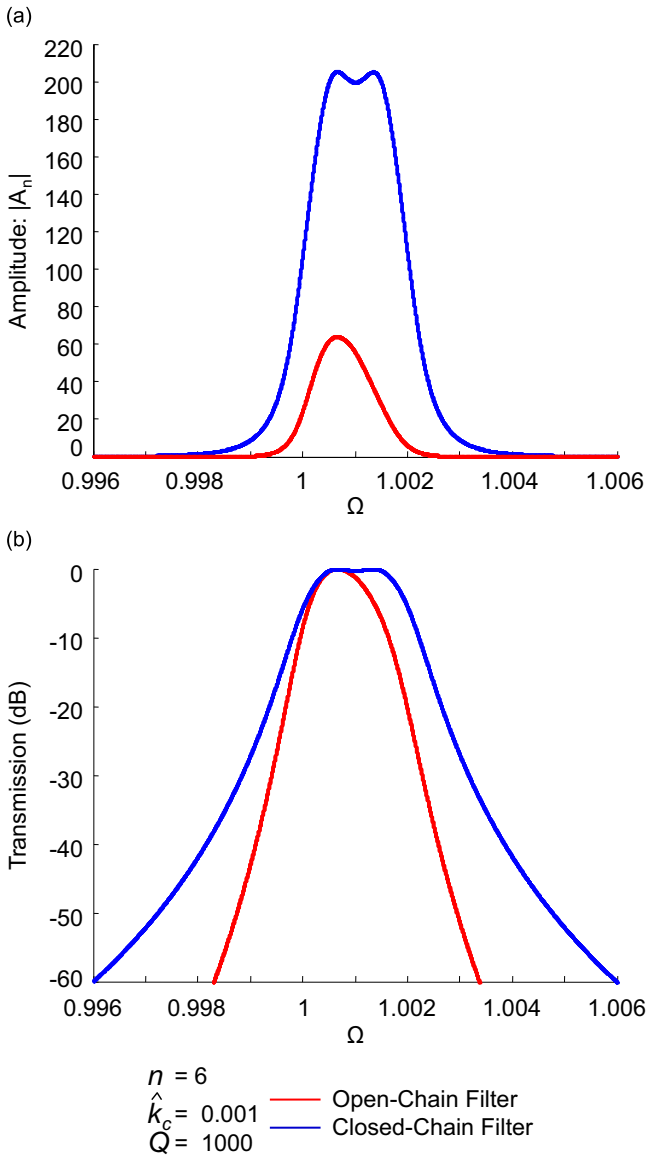

Fig. 6. Response amplitude (a) and transmission (b) for 6-resonator, open- and closed-chain filters, respectively.

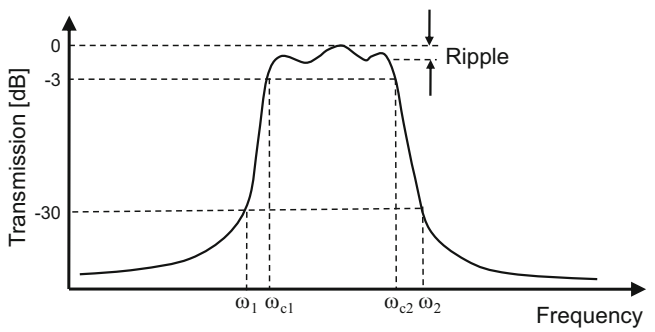

Fig. 7. Frequency response of a real filter.

- Shape factor (SF) (referenced to 30 dB attenuation) $=(\omega_2-\omega_1)/(\omega_{c2}-\omega_{c1})$,
- Minimum insertion loss (IL) (in dB) $=20\log_{10}(1/A_{\max})=-20\log_{10}(A_{\max})$.

In most filter implementations, high effective quality factors, near-unity shape factors, and minimal insertion loss are desired.

3. The performance of filters composed of identical resonators

As previously noted, the model developed herein is independent of the geometric/structural design of a given filter. As a result, by assuming that the filter's constituent resonators and coupling elements are identical and that dissipative coupling is negligible to first order, a given filter can be parameterized solely by the number of resonators in the array (n), the elastic coupling coefficient ($\hat{k}_c$), and the isolated resonator's quality factor (Q). As the relationship between these parameters and pertinent filter metrics cannot be obtained in a tractable closed form for arbitrary n, numerical computations are performed over a wide, yet feasible, design space to investigate this dependency. The design space considered here spans $\hat{k}_c$ values from 0.0001 to 0.1 and Q values from 100 to 10^6 and the filter metrics are evaluated at 121×161 grid points, which are uniformly distributed (in log scale) across the space. The analysis is performed for open- and closed-chain filters for even n values varying from 6 to 16. Pertinent results are summarized here. In all of the reported results, it should be noted that the filter designs exhibiting a ripple magnitude in excess of 3 dB within the passband have been deemed unsuitable for practical implementation (as they induce more than 50 percent signal attenuation). These points are flagged with dark red color in the contour plots and are omitted from subsequent analysis.

While the relationship between the filter design parameters delineated above and pertinent filter metrics are fairly well understood for open-chain filter architectures, these relationships are yet to be fully characterized for cyclically coupled systems. In an attempt to help remedy this deficiency Fig. 8 details the effective quality factor (EQF) metrics associated with a 6-resonator, closed-chain filter across a reduced parameter space which excludes the region beyond $Q=10^{4.5}$ and $\hat{k}_c=10^{-1.5}$, where ripple in excess of 3 dB is present. Not surprisingly, Fig. 8 reveals that higher EQF can be obtained by minimizing $\hat{k}_c$ and maximizing Q. Less intuitive, however, is the fact that the level curve associated with a particular EQF spans appreciable portions of the feasible design space. Three level curves (constructed from a small subset of data-points) corresponding to EQFs of 1000, 2000 and 4000, respectively, are shown in Fig. 8. Interestingly, if one traverses these level curves from point A through E_1 to point E_{10}, from point F through J_1 to point J_{10}, and from K through O_1 to point O_{10}, one notices both a monotonic decrease in shape factor (referenced to 30 dB) [Fig. 9(a)] and a monotonic decrease in minimum insertion loss [Fig. 9(b)]. However, the ripple, not present until points E_1, J_1, and O_1 (while traversing from left to right), increases quite rapidly through points E_{10}, J_{10} and O_{10}, as shown in Fig. 9(c). Accordingly, for designs founded upon a particular EQF value, a clear trade-off is observed between shape factor and insertion loss on one hand, and ripple on the other.

Studying the filter metrics of a 6-resonator closed-chain filter, helps to identify three distinct design regions, which are highlighted in the contour plot of ripple in Fig. 10:

- Region (A) with a single peak in the frequency spectrum: The response in this region features a very broad peak with high insertion loss. Filters based on (or operating in) this region feature poor frequency selectivity.

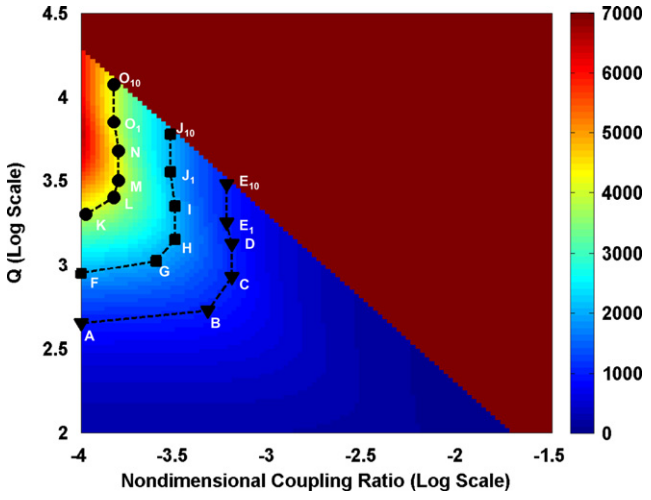

Fig. 8. Contour plot depicting the effective quality factor (EQF) for a 6-resonator, closed-chain filter. Note that here, and in the work's other figures, nondimensional coupling ratio refers to the nondimensional elastic coupling coefficient $\hat{k}_c$.

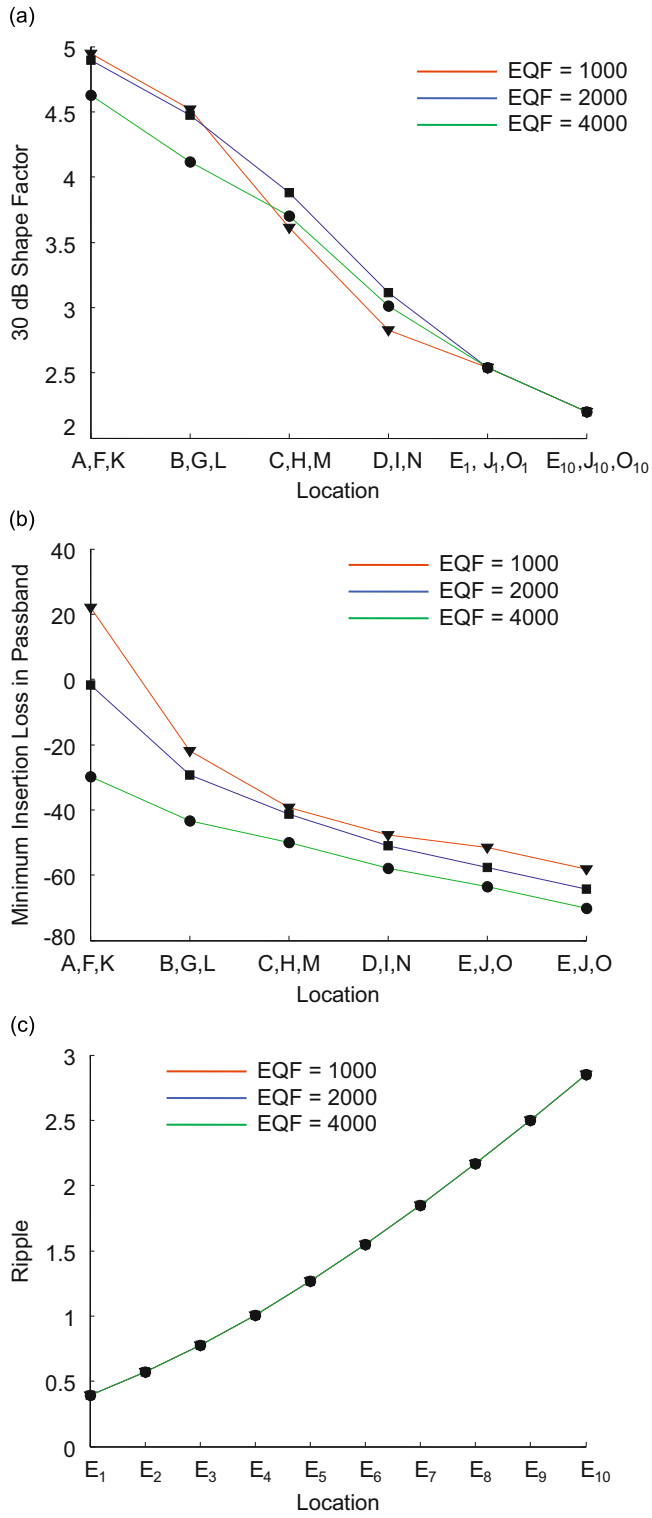

Fig. 9. (a) Shape factor acquired at the data-points labeled in Fig. 8 computed with respect to a 30 dB reference. (b) Minimum insertion loss recovered at the data-points labeled in Fig. 8. (c) Ripple recovered at data-points E_1–E_{10}, J_1–J_{10}, and O_1–O_{10}. Note that the ripple trajectories are nearly identical in this parameter space.

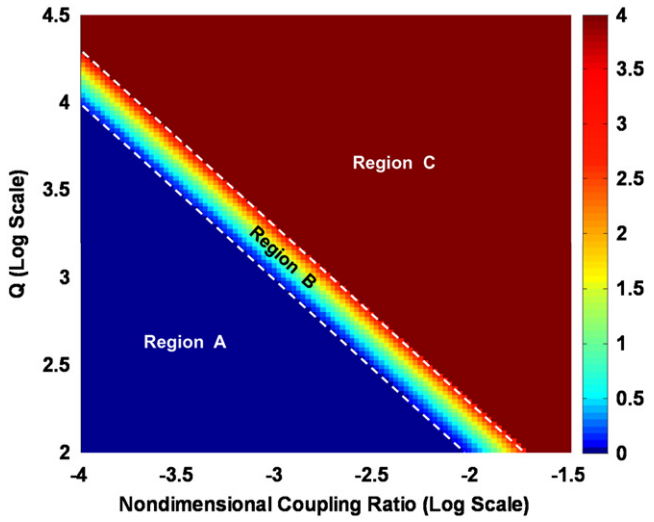

Fig. 10. Contour plot depicting the magnitude of ripple (dB) for a 6-resonator, closed-chain filter.

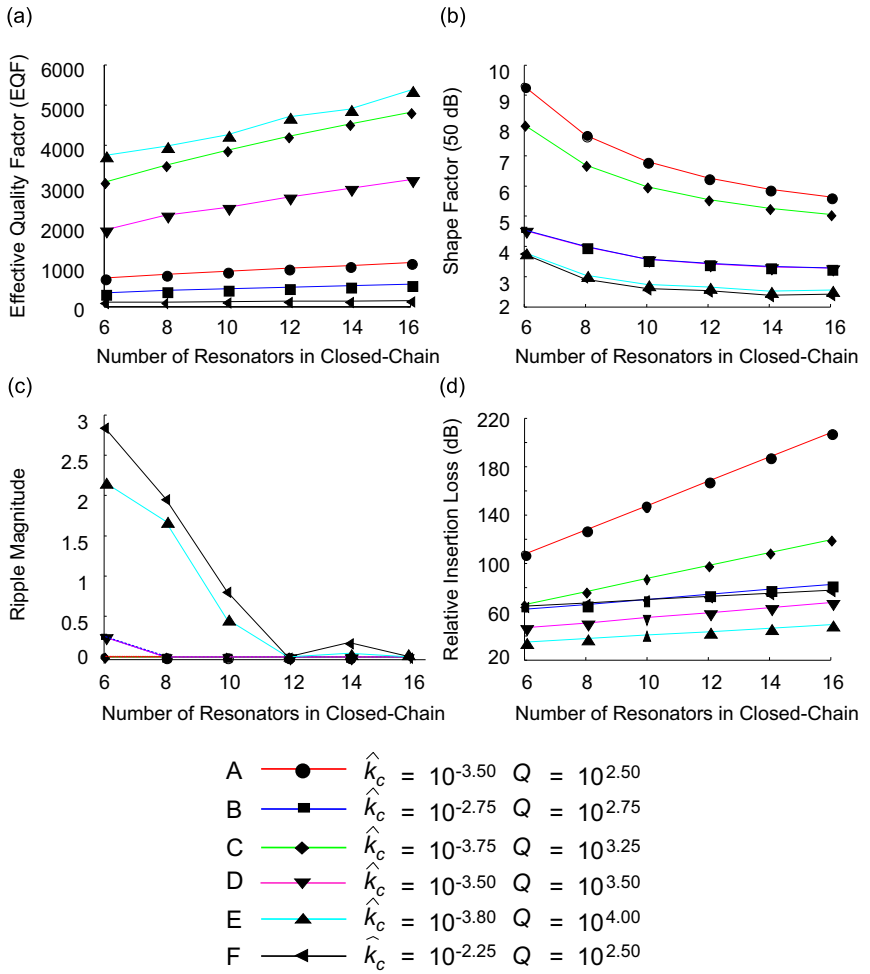

Fig. 11. (a) EQF, (b) SF (referenced to 50 dB), (c) ripple, and (d) minimum insertion loss acquired at the indicated data-points with a varying number of resonators in the filter.

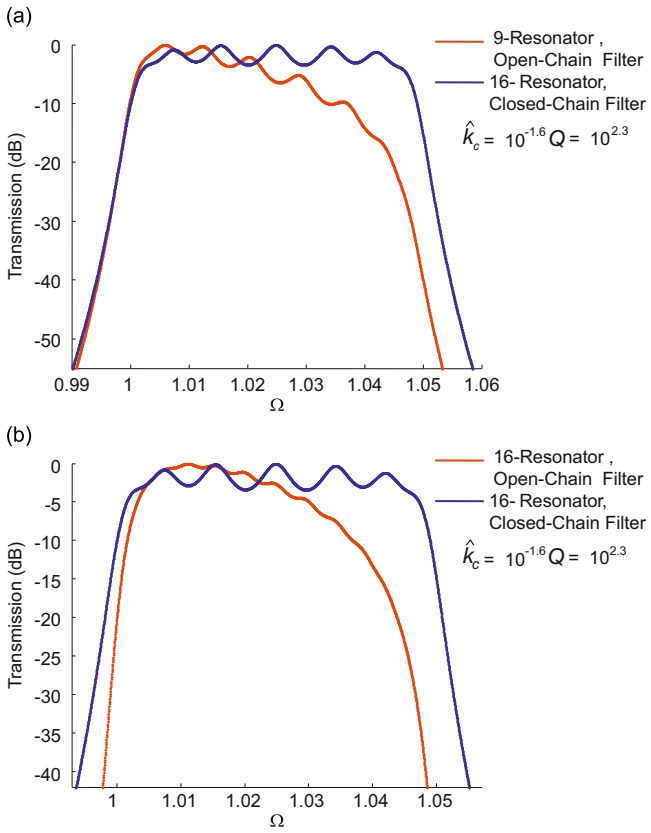

Fig. 12. Transmission characteristics of open- and closed-chain, higher-order filters.

- Region (B) containing two peaks in the frequency spectrum: The response in this region features a ripple between 0 and 3 dB and possesses comparatively superior EQF and SF and minimum IL. However, the presence of ripple results in an amplitude variation of up to 50 percent in the passband.
- Region (C): The response in this region possesses either two or four peaks with a ripple magnitude greater than 3 dB. Due to the imposed constraint on the ripple magnitude, a filter should not be designed (or operated) in this region.

From the summary above, it is clear that a filter design operating in Region (B) is ideal for attaining superior filter metrics. This can be achieved through both proper *a priori* design and post-fabrication Q and $\hat{k}_c$ manipulation, accomplished through tuning and/or packaging.

3.1. Results for higher-order, closed-chain filters

Conventional filter theory dictates that pertinent performance metrics can often be improved by increasing the filter's effective order. To this end, numerical simulations similar to those detailed above are repeated for even values of n ranging from 8 to 16. Recovered filter metrics are then compared at a few distinct points (A–F), which were randomly chosen in the 2D design space, as presented in Fig. 11. It is evident that while the EQF increases and shape factor (referenced to 50 dB here) and ripple decrease with n, the minimum insertion loss increases drastically with the number of resonators in the chain. Thus, as in classical filter design, a clear trade-off is observed between filters with higher effective quality factor, selectivity, and lower ripple on one hand, and an increased insertion loss on the other.

3.2. Comparison of open- and closed-chain filters

In order to develop a clear declaration on the relative utility of cyclically coupled filter designs, it is prudent to benchmark these devices against their open chain counterparts with both n and $n/2+1$ resonators (the latter is due to the degeneracy of the closed-chain architecture's eigenstructure). Fig. 12 presents a snapshot of this comparison by highlighting the transmission characteristics of a 16-resonator, closed-chain filter, a 16-resonator open-chain filter, and a 9-resonator, open-chain filter. It is seen that in the open-chain case, starting with the second peak, there is a monotonic

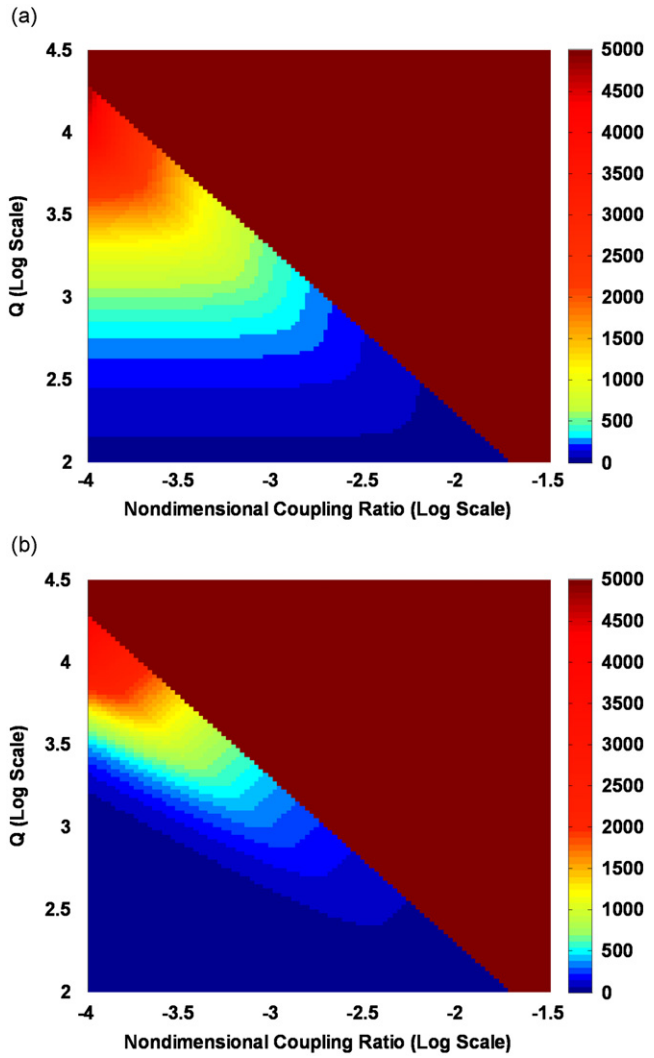

Fig. 13. Contour plots depicting the difference between the effective quality factors associated with: (a) 6-resonator, open-chain and 6-resonator, closed-chain and (b) 4-resonator, open-chain and 6-resonator, closed-chain designs.

decay in the super-imposed ripple, which accentuates with an increase in the number of elements. Though this results in a smaller bandwidth for higher-order filters, the passband does not encompass the entire resonance region, resulting in filters with poor selectivity, a nonsmooth transition band, and an asymmetric frequency response. The closed-chain filters, on the other hand, exhibit a nominally symmetric response (about the center frequency) with higher transmission, and a bandwidth and ripple magnitude which decrease with additional resonators in the chain. This results in a more selective filter with a higher quality factor and smooth transition band. As such, for devices composed of identical resonators, while higher-order filters based on open-chain architecture seem to deviate from the ideal bandpass filter characteristic, the ones based on closed-chain architecture approach it (refer to Fig. 12)!

Fig. 13 shows the difference in effective quality factor (EQF) for open- and closed-chain filters. The comparison of 6-resonator, closed-chain is made with 6-, as well as 4-, resonator open-chain designs, see Fig. 13. As evident, open-chain filters offer higher EQF when compared to their closed-chain counterparts, with the difference being accentuated when comparing with a 6-resonator, open-chain filter design. As noted earlier, for an open-chain, only a portion of the resonance region is contained within the passband due to its decay with increasing frequency, and thus a narrower bandwidth is obtained. As such, the difference between an open- and closed-chain filters' EQF is expected to increase with a higher number of resonators in the chain.

Fig. 14 shows the difference in 10 dB shape factor (SF) between open- and closed-chain filters. As noted earlier, closed-chain filters are more selective throughout the design domain and this difference is accentuated when comparing, 6-resonator closed- and open-chain filters. While the difference is comparatively small with very low levels of coupling and Q, in region B (noted earlier to be the most favorable region to design closed-chain filters) this difference is quite high.

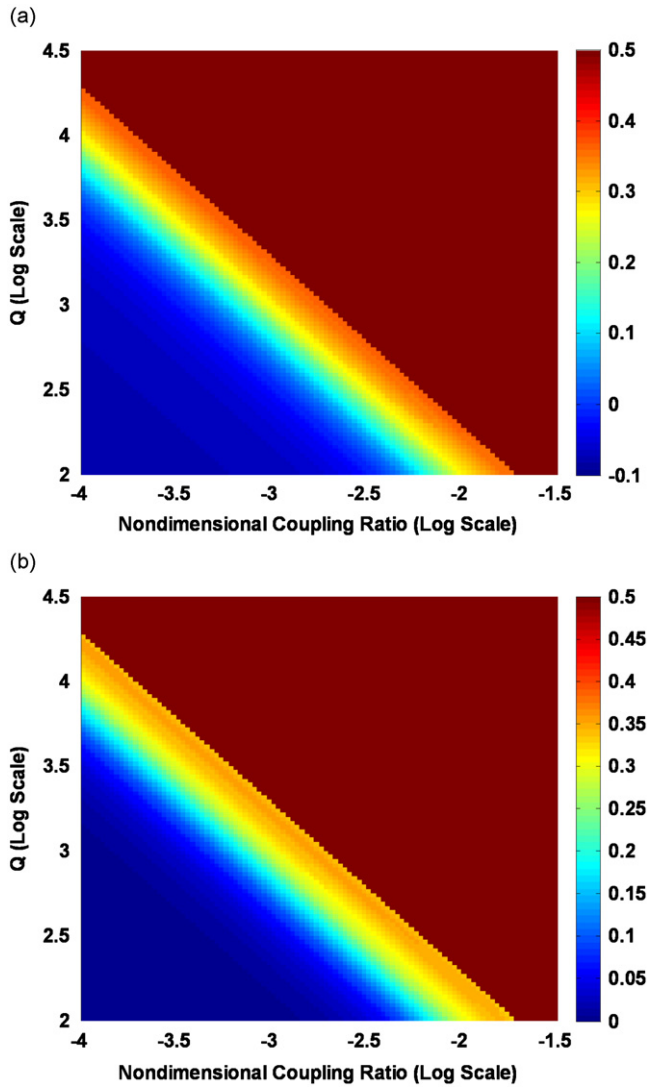

Fig. 14. Contour plots depicting the difference between the shape factors (referenced to 10 dB) associated with: (a) 6-resonator, open-chain and 6-resonator, closed-chain and (b) 4-resonator, open-chain and 6-resonator, closed-chain designs.

4. The effect of process-induced variation on filter performance

The simulation results presented in the earlier sections of this work were based on the assumption that all the resonators, as well as coupling elements, in the open- and closed-chain filter designs are nominally identical and that resonant frequencies could be specified exactly. However, owing to many practical constraints, such as dimensional and material property variations, and residual stresses, this is impossible to achieve. Generally speaking, fabrication uncertainty is regarded as one of the key roadblocks in the commercialization of MEMS devices [17], given that it can lead to tolerances higher than ± 10 percent of the nominal design and large deviations in performance [18]. While post-fabrication laser trimming [18], voltage bias tuning [4,19,20] and localized thermal stressing [21] can be used to correct for these variations, the cost and the effort involved in individually tuning/trimming renders a need for inherently robust device designs. This section attempts to quantify the impact of process-induced variations by investigating and comparing the robustness offered by both open-chain and closed-chain filter architectures. To this end, deviations in the masses and stiffnesses of the individual resonators are modeled as variations in the nondimensional stiffness ratio $\hat{k}_i$, elastic coupling ratio $\hat{k}_c$, and mass $\hat{m}_i$ and Monte Carlo simulations [22] are performed to characterize performance.

As the elastic coupling ratio $\hat{k}_c$ (10^{-5}–10^{-1}) is orders of magnitude smaller than the nondimensional stiffness $\hat{k}_i$ and mass $\hat{m}_i$ (nominally equal to unity), a small percentage variation in $\hat{k}_i$ or $\hat{m}_i$ would overshadow the effect of variations in $\hat{k}_c$. Accordingly, the effects of process-induced variations are studied in two stages. In the first stage, variations in the elastic

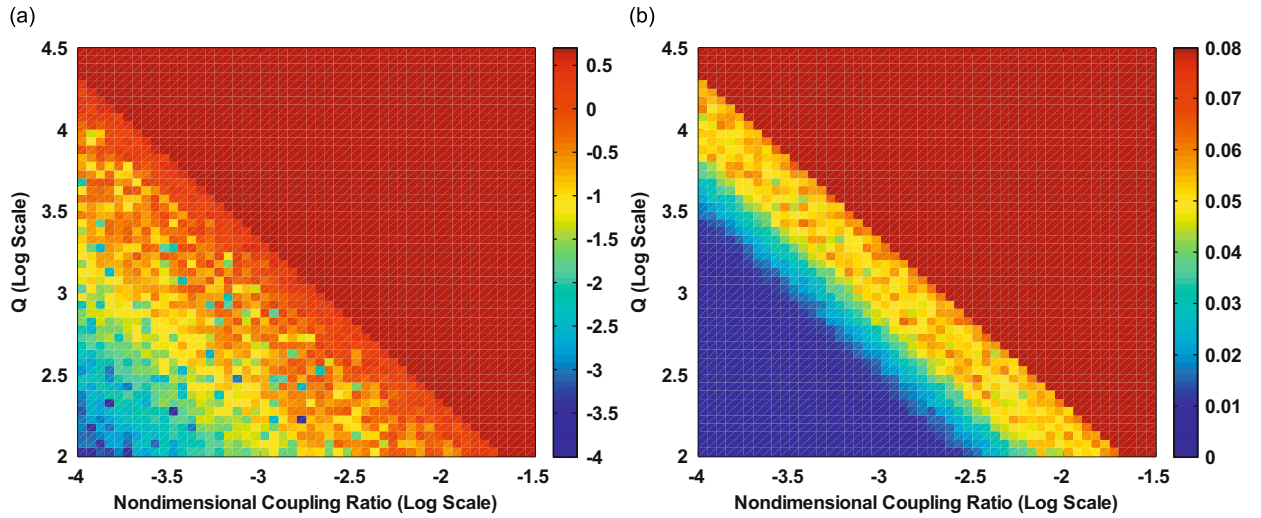

Fig. 15. (a) Mean percentage error in log scale and (b) normalized standard deviations in BW for 6-resonator, closed-chain filters with ± 20 percent random variation in $\hat{k}_c$.

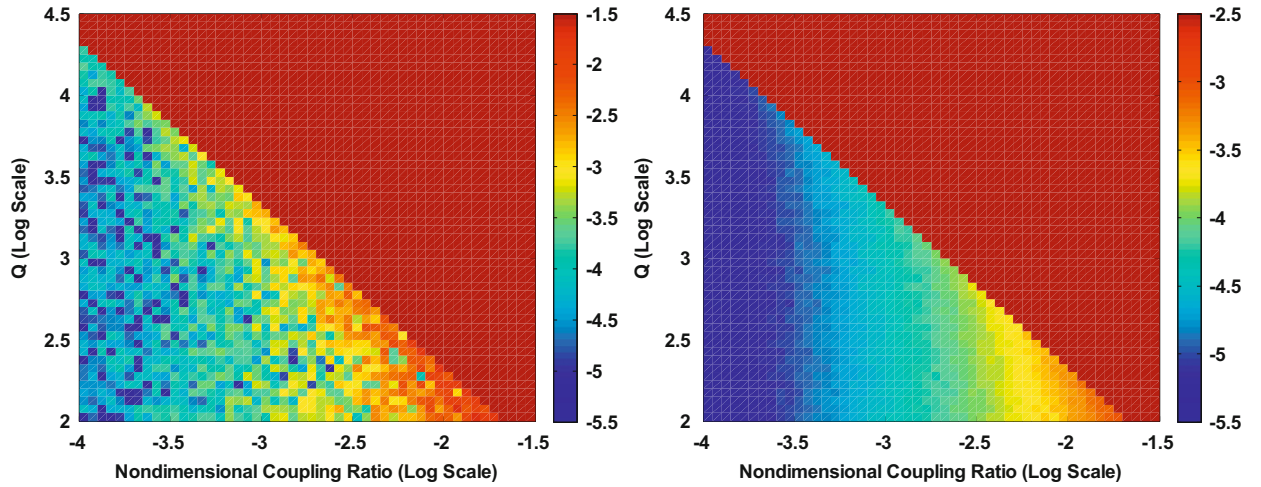

Fig. 16. (a) Mean percentage error and (b) normalized standard deviations in CF for 6-resonator, closed-chain filters with ± 20 percent random variation in $\hat{k}_c$ (shown in log scale).

coupling ratio $\hat{k}_c$ are considered independently. In the second stage, the combined effect of variations in $\hat{k}_i$, $\hat{m}_i$, and $\hat{k}_c$ is investigated. Given the stochastic nature of this analysis, simulations are repeated until sufficient convergence is achieved in both center frequency (CF) and bandwidth (BW). Here the degree of convergence is founded upon the criteria that the mean percentage error associated with both of these quantities do not vary, across the feasible design space, by more than 0.01 percent (first stage) and 0.5 percent (second stage) of its value with the inclusion of one additional simulation. In both scenarios, 400 simulations yielded sufficient convergence.

As the focus here is to analyze deviation from a nominal filter design, the results are presented in terms of both mean percentage error (compared to the nominal case) and normalized standard deviation in the center frequency CF and the bandwidth BW. These quantities are defined as follows:

- Mean error percentage in CF:

$$Z_1(\hat{k}_c, Q) = \frac{\left|\frac{1}{N}\sum_{i=1}^{N}(\mathrm{CF}_i) - \mathrm{CF}_{\mathrm{nom}}\right|}{\mathrm{CF}_{\mathrm{nom}}} \times 100 \text{ percent},$$

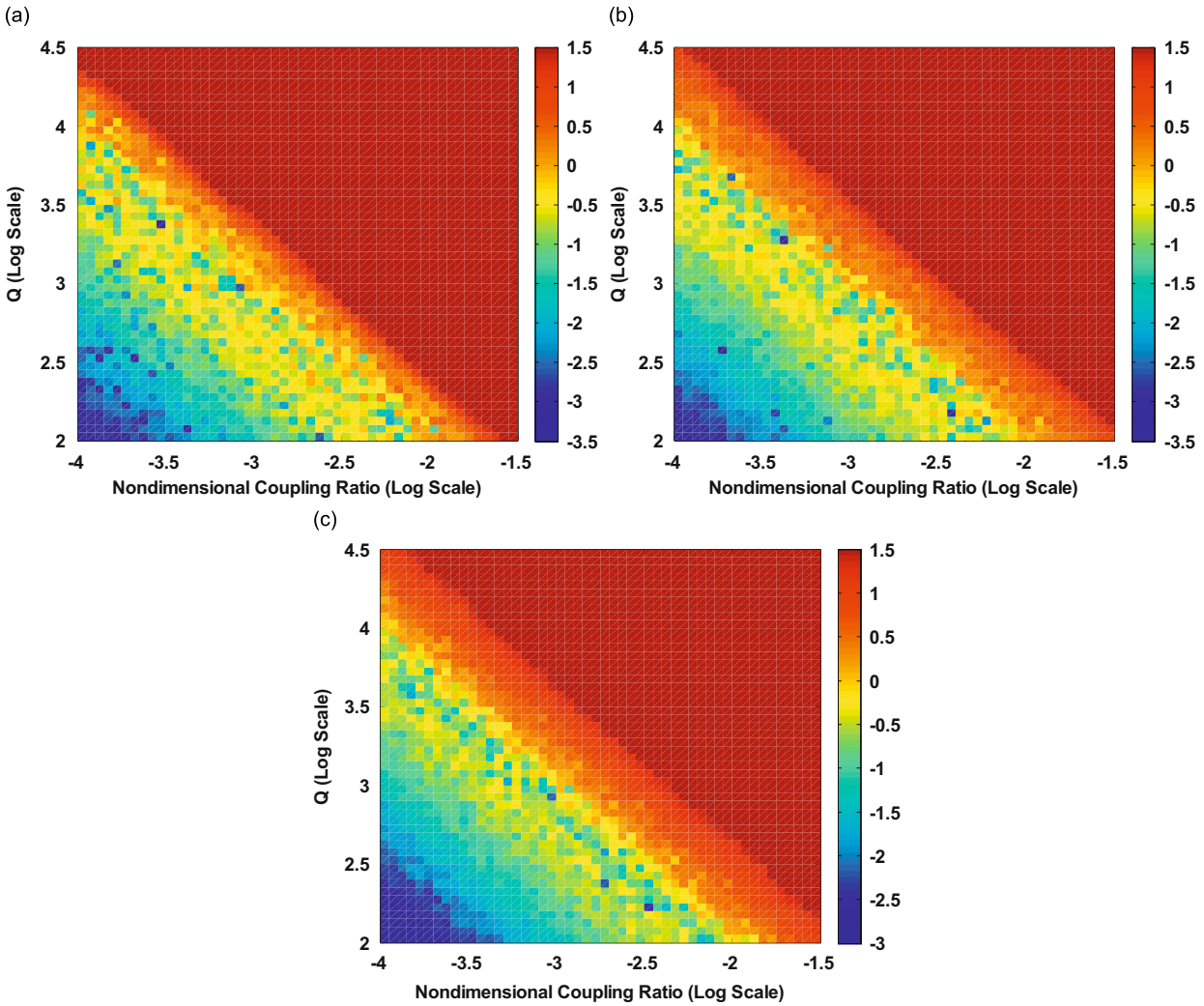

Fig. 17. Mean percentage error in BW (log scale) with ± 20 percent random variation in $\hat{k}_c$ for (a) $n=8$, (b) $n=12$, and (c) $n=16$.

- Normalized std. deviation in CF:

$$Z_2(\hat{k}_c,Q) = \frac{\sqrt{\frac{1}{N}\sum_{i=1}^{N}(\mathrm{CF}_i - \overline{\mathrm{CF}})^2}}{\overline{\mathrm{CF}}},$$

- Mean error percentage in BW:

$$Z_3(\hat{k}_c,Q) = \frac{\left|\frac{1}{N}\sum_{i=1}^{N}(\mathrm{BW}_i) - \mathrm{BW}_{\mathrm{nom}}\right|}{\mathrm{BW}_{\mathrm{nom}}} \times 100 \text{ percent},$$

- Normalized std. deviation of BW:

$$Z_4(\hat{k}_c,Q) = \frac{\sqrt{\frac{1}{N}\sum_{i=1}^{N}(\mathrm{BW}_i - \overline{\mathrm{BW}})^2}}{\overline{\mathrm{BW}}}.$$

Note N is the number of simulations (to be distinguished from the number of resonator in the filter n), CF_i and BW_i are the center frequency and bandwidth of ith simulation iteration, and $\overline{\mathrm{CF}}$ and $\overline{\mathrm{BW}}$ are the mean center frequency and bandwidth values, as computed using the entirety of the Monte Carlo simulation.

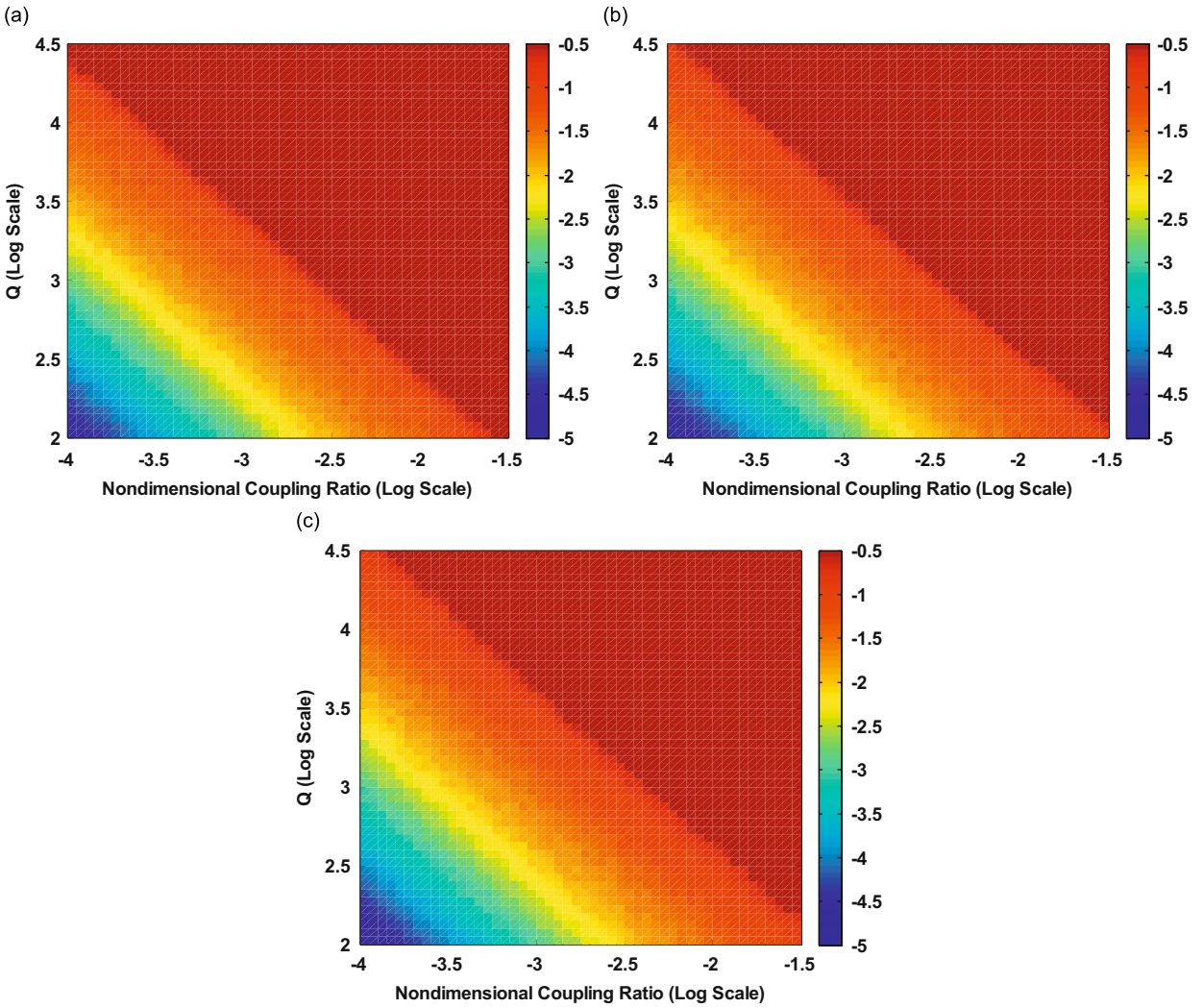

Fig. 18. Mean percentage error in CF (log scale) at ± 20 percent random variation in $\hat{k}_c$ for (a) n=8, (b) n=12, and (c) n=16.

4.1. *Variations in* $\hat{k}_c$

Fig. 15 highlights the variation in mean percentage error and normalized standard deviation in bandwidth BW (MEBW and SDBW, respectively) across the design space for a 6-resonator, closed-chain filter with ± 20 percent variation in $\hat{k}_c$. From the contour plot, it is seen that the mean error as well as the standard deviations are higher at design points that are closer to the 3 dB ripple boundary and vary roughly as a product of $\hat{k}_c$ and Q. The mean error in bandwidth (MEBW) is seen to be less than 3.98 percent throughout the feasible design space and the standard deviation is seen to be less than 0.06 times its nominal value. Vibration localization is evident in the design space (see Fig. 15), as revealed by the nonuniform and abrupt changes in the mean values at certain locations and inspection of isolated frequency responses.

Fig. 16 shows the variation in the mean percentage error and normalized standard deviation in center frequency (MECF and SDCF, respectively) across the feasible design space for a 6-resonator, closed-chain filter with ± 20 percent variation in $\hat{k}_c$. Unlike bandwidth, center frequency is primarily a function of $\hat{k}_c$. For a closed-chain filter with an even number of resonators, it is approximately equal to $1+\hat{k}_c$ (see [23]). Hence, the error varies primarily as a function of $\hat{k}_c$ (see Fig. 16). The mean error in CF is seen to be less than 0.02 percent throughout the feasible design space with a standard deviation less than 0.001 times its mean value.

Figs. 17 and 18 present the MEBW and MECF contour plots for 8-, 12- and 16-resonator, closed-chain filters with ± 20 percent variation in $\hat{k}_c$. The mean errors in bandwidth as well as center frequency are seen to increase significantly for higher-order, closed-chain filters. For example, at ± 20 percent variation in $\hat{k}_c$, while the maximum mean error in BW is

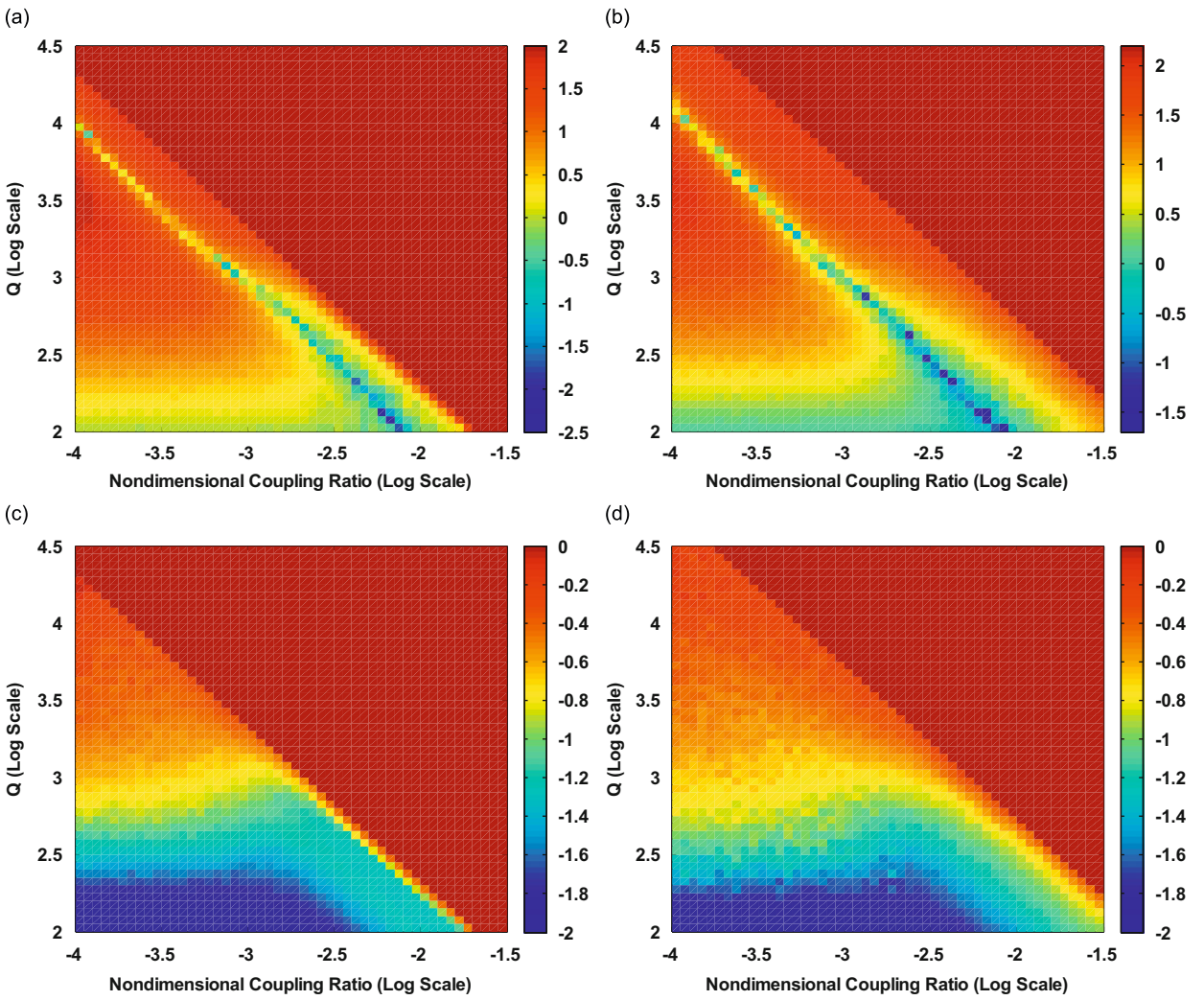

Fig. 19. Mean percentage error (log scale) in BW for (a) 6-resonator, and (b) 16-resonator, closed-chain filters. Normalized standard deviations (in log scale) in BW for (c) 6-resonator and (d) 16-resonator, closed-chain filters.

3.98 percent for a 6-resonator, closed-chain filter, it increases to 5.49, 11.32 and 17.49 percent, respectively, for, 8-, 12- and 16-resonator filters. Similarly, the maximum error in center frequency increases 10-fold from 0.0235 percent (for a 6-resonator filter) to 0.2315 percent (for a 16-resonator filter). This, not surprisingly, reveals that higher-order filters are more sensitive to variations amongst the resonators, due to the increased potential for such variations to occur.

4.2. *Variations in $\hat{k}_i$, $\hat{k}_c$ and $\hat{m}_i$*

To buttress the results of the previous subsection, simulations were initiated that considered variations in nondimensional mass and stiffness ratio up to ± 0.1 percent of the nominal values and variations in $\hat{k}_c$ up to ± 20 percent. Fig. 19 shows the mean error in bandwidth (MEBW) for 6-resonator (a), and 16-resonator (b), closed-chain filters with the aforementioned variations. For the 6-resonator filter, while the maximum error in BW is observed as high as 77 percent, the error through most of the feasible design space is less than 30 percent. It is interesting to note that in the neighborhood of design points satisfying $\hat{k}_c \times Q = 1$ (approximately), the difference between the bandwidth of the nominal case $\mathrm{BW}_{\mathrm{nom}}$ and the mean bandwidth of the simulation iterations $\overline{\mathrm{BW}}$ changes sign from negative to positive, thus indicating a very low percentage error in bandwidth. Note that, similar trends are observed for all n (from 6 through 16). As such, filters designed in this region are expected to be the least sensitive to variations amongst the resonators. Fig. 20 shows the mean error and normalized standard deviation in center frequency (respectively) for 6-resonator and 16-resonator, closed-chain filters for the variation levels delineated above. For the

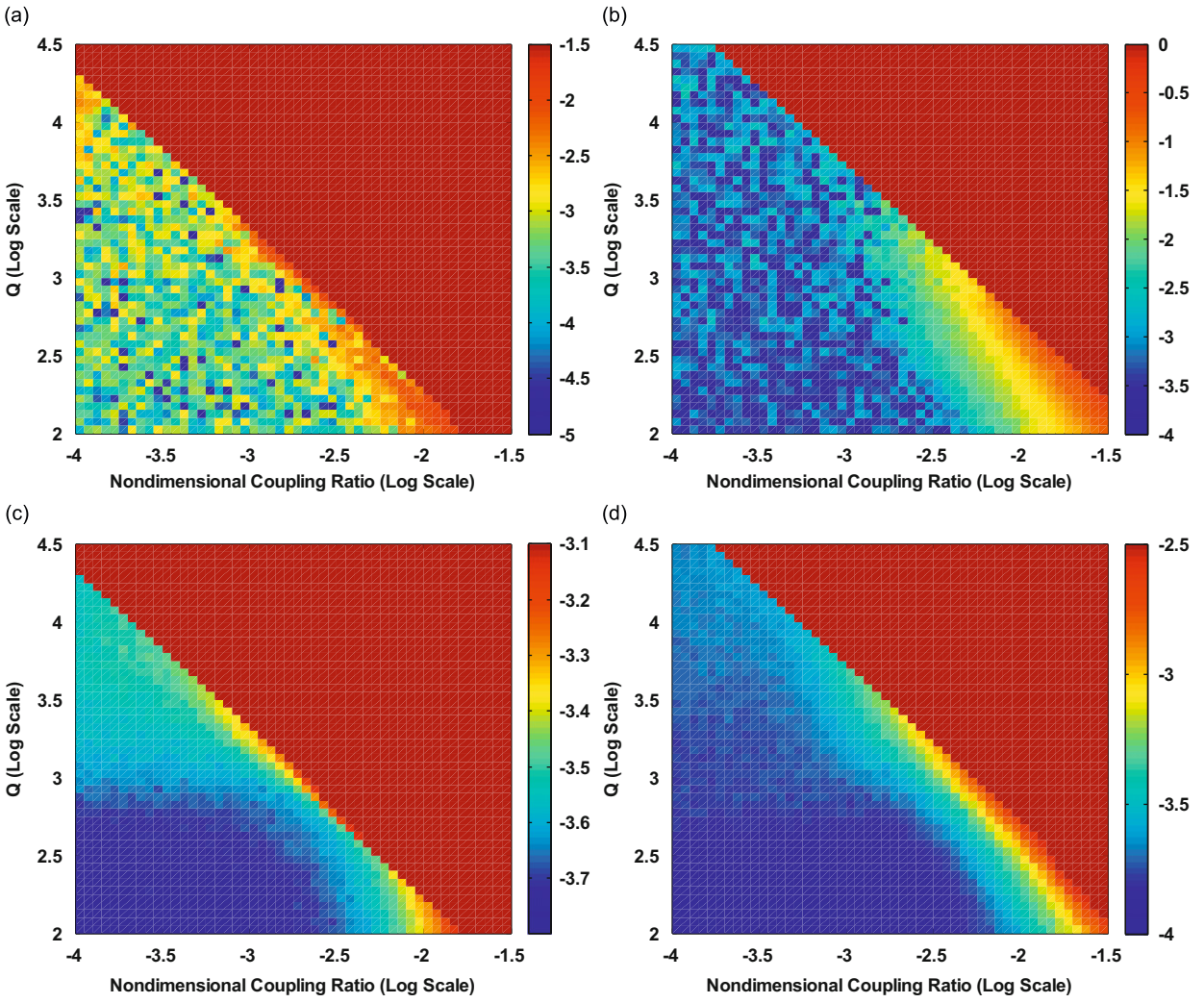

Fig. 20. Mean percentage error (log scale) in CF for (a) 6-resonator, and (b) 16-resonator, closed-chain filters. Normalized standard deviations (in log scale) in CF for (c) 6-resonator and (d) 16-resonator, closed-chain filters.

6-resonator filters, while the maximum error in CF is observed as high as 1.25 percent, the error through most of the feasible design space is less than 0.06 percent. The error values and standard deviations are relatively higher for the 16-resonator filters.

4.3. Comparison with open-chain filters

Given that the absolute performance bounds developed in the preceding sections provide little insight on the *relative* robustness of closed-chain filter architectures, comparisons are made between the mean errors in bandwidth and center frequency associated with both open- and closed-chain filter architectures. As before, Monte Carlo simulation are performed with random variations up to ± 0.1 percent in $\hat{k}_i$ and $\hat{m}_i$, and up to ± 20 percent in $\hat{k}_c$, until sufficient convergence has been achieved. The results of these simulations are presented here as the difference between MEBW and MECF values for open- and closed-chain filters. Note that for the sake of completeness, the results obtained for 4-resonator open-chain filters are compared with those for 4-resonator and 6-resonator, closed-chain filter designs.

Fig. 21 presents the difference of mean errors and normalized standard deviations in bandwidth for open- and closed-chain filters. The closed-chain filters are seen to be more robust through most of the feasible design space (indicated by the positive difference) barring a thin strip of dark-blue region, as shown in Fig. 21. With the magnitude of variations considered, the open-chain filter has a mean error as high as 304 percent in the common feasible design space. The

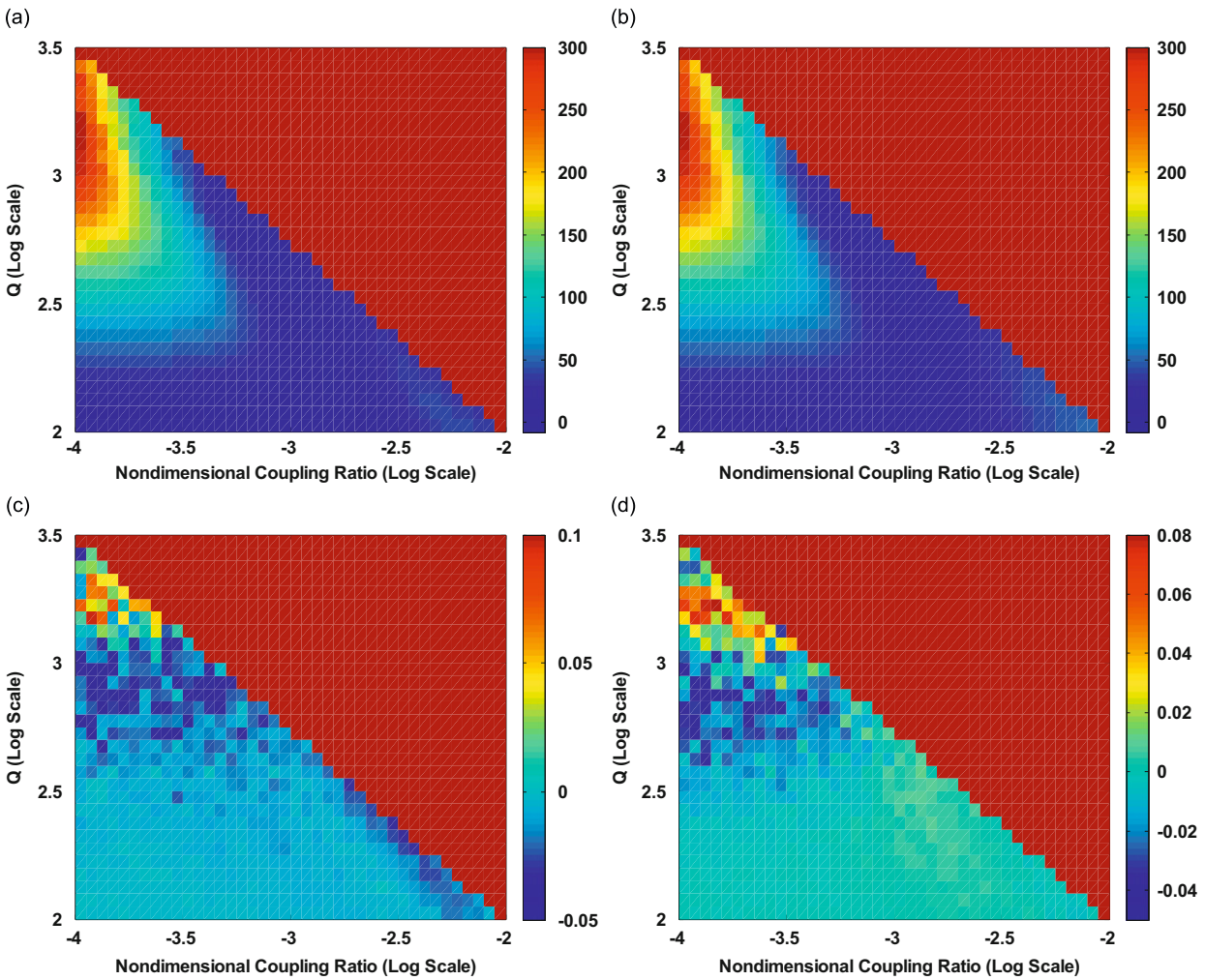

Fig. 21. Difference between mean errors in bandwidth of (a) 4-resonator, open- and closed-chain and (b) 4-resonator, open- and 6-resonator, closed-chain filter designs. Difference between normalized standard deviations in BW of (c) 4-resonator, open- and closed-chain and (d) 4-resonator, open- and 6-resonator, closed-chain filter designs.

normalized standard deviations, however, are of comparable magnitudes indicated by the positive as well as negative values in the feasible design space.

Fig. 22 presents the difference of mean errors and normalized standard deviations in center frequency for open- and closed-chain filters. The difference in mean errors is seen to be positive through most of the feasible design space indicating that closed-chain filters are generally more robust than their open-chain counterparts, with respect to the center frequencies also. The limited region with negative difference has relatively low magnitude (less than 0.006) compared to the magnitude of positive difference. The values of standard deviations are also lower for the closed-chain filters through most of the feasible design space, further establishing their superior robustness.

Collectively, Figs. 21 and 22 indicate that closed-chain filter designs are more robust to variations amongst the resonators. Thus, in practice, filters based on these designs should require less frequency tuning or post-processing, as compared to those designs based upon conventional, open-chain filter architectures.

5. Conclusion

In this paper, bandpass filters based on nontraditional, cyclic coupling architectures were modeled and analyzed. Lumped-parameter modeling was used to capture the salient dynamics of open- and closed-chain filter designs which were parameterized by a nondimensional coupling ratio and an isolated resonator quality factor. The response of filters composed of identical resonators were then analyzed over a wide, yet realistic, range of these parameters, and the

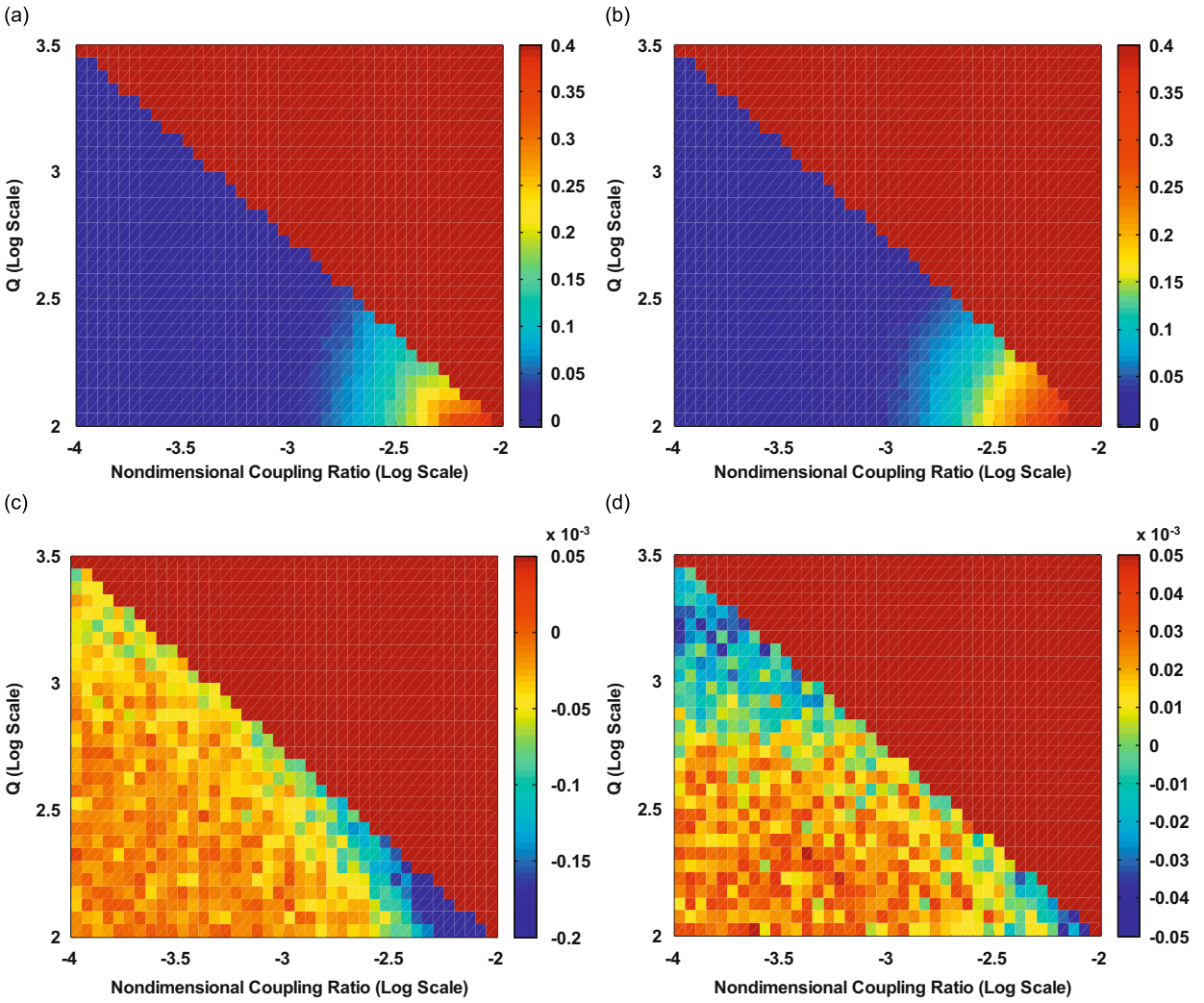

Fig. 22. Difference between mean errors in center frequency of (a) 4-resonator, open- and closed-chain and (b) 4-resonator, open- and 6-resonator, closed-chain filter designs. Difference between normalized standard deviations in CF of (c) 4-resonator, open- and closed-chain and (d) 4-resonator, open- and 6-resonator, closed-chain filter designs.

performance metrics associated with the closed-chain architecture were benchmarked against conventional, open-chain filter designs. The closed-chain filters were found to be generally more selective, with steeper roll-offs, lower ripple magnitudes and more symmetric passbands, as compared to the open-chain filter designs. Additionally, it was determined that the passbands of open-chain filters operating at a majority of points in the feasible design space, failed to encompass the entire resonance region. This led to poor selectivity, a nonsmooth transition band, and an asymmetric frequency response. In contrast, higher-order, closed-chain filters were found to exhibit good selectivity metrics with lower ripple, but at the expense of an increased insertion loss.

The effect of process-induced variation on the performance of closed- and open-chain filters was investigated by introducing variations in the nondimensional coupling and damping parameters, and performing Monte Carlo simulation throughout the feasible design space. The error in performance metrics, characterized by a mean percentage error and normalized standard deviation in the bandwidth and center frequency, was generally found to be lower for closed-chain filters as compared to open-chain filters, indicating that the architecture is likely more robust to process-induced variations. Though implementable, closed-chain filters will likely require some degree of frequency tuning, the above result is very useful in light of the cost and effort involved with post-processing in a mass production setting.

Current efforts are aimed at developing device-specific multi-physics models, device fabrication, and experimental validation. Fig. 23 highlights some of the initial filter designs under development. These filters utilize an out-of-plane flexural mode of vibration and have center frequencies ranging from approximately 10 kHz to 5 MHz.

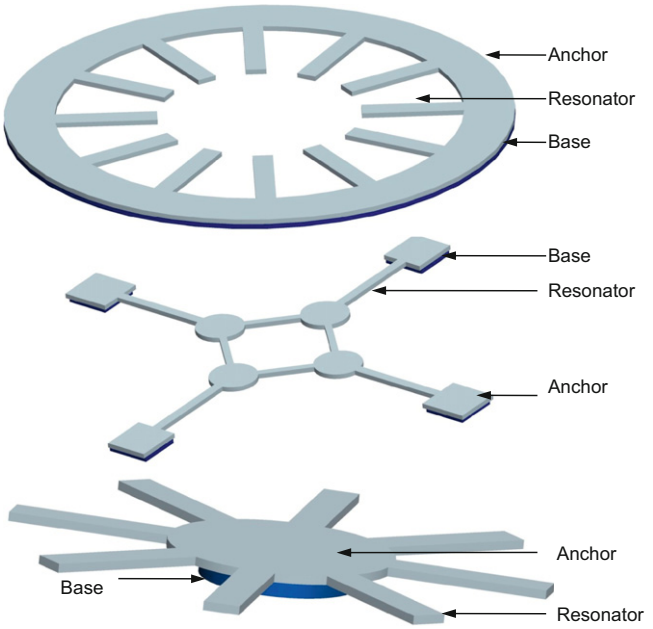

Fig. 23. Preliminary closed-chain filter designs.

Acknowledgments

This work was graciously supported by the National Science Foundation (NSF) under Grant NSF-0846385 and Purdue University.

References

[1] H.A.C. Tilmans, W. DeRaedt, E. Beyne, MEMS for wireless communications: 'from RF-MEMS components to RF-MEMS-SiP', *Journal of Micromechanics and Microengineering* 13 (2003) 139–163.
[2] J.N. Burghartz, Status and trends of silicon RF technology, *Microelectronics Reliability* 1 (2001) 13–22.
[3] J.J. Yao, RF MEMS from a device perspective, *Journal of Micromechanics and Microengineering* 10 (2000) 9–38.
[4] C.T.-C. Nguyen, Micromechanical resonators for oscillators and filters, *Technical Digest of the IEEE Ultrasonics Symposium*, Seattle, 1995, pp. 489–499.
[5] F.D. Bannon III, J.R. Clark, C.T.-C. Nguyen, High frequency microelectromechanical IF filters, *Technical Digest of the IEEE Electron Devices Meeting*, San Francisco, 1996, pp. 773–776.
[6] Y. Xie, S.-S. Li, Y.-W. Lin, Z. Ren, C.T.-C. Nguyen, UHF micromechanical extensional wine-glass mode ring resonators, *Technical Digest of the IEEE International Electron Devices Meeting*, Washington, 2003, pp. 953–956.
[7] M.U. Demirci, C.T.-C. Nguyen, Mechanically corner-coupled square microresonator array for reduced series motional resistance, *Journal of Microelectromechanical Systems* 15 (2006) 1419–1436.
[8] L. Lin, R.T. Howe, A.P. Pisano, Microelectromechanical filters for signal processing, *Journal of Microelectromechanical Systems* 7 (1998) 286–294.
[9] M. Motiee, R.R. Mansour, A. Khajepour, Novel MEMS filters for on-chip transceiver architecture, modeling and experiments, *Journal of Micromechanics and Microengineering* 16 (2006) 407–418.
[10] D.S. Greywall, P.A. Busch, Coupled micromechanical drumhead resonators with practical application as electromechanical bandpass filters, *Journal of Micromechanics and Microengineering* 12 (2002) 925–938.
[11] B. Piekarski, D. DeVoe, M. Dubey, R. Kaul, J. Conrad, R. Zeto, Surface micromachined piezoelectric resonant beam filters, *Sensors and Actuators A* 91 (2001) 313–320.
[12] M. Zhu, P.B. Kirby, High-Q micro-machined piezoelectric mechanical filters using coupled cantilever beams, *Proceedings of SPIE, Smart Sensors, Actuators, and MEMS*, Seville, 2005, pp. 516–526.
[13] K. Wang, C.T.-C. Nguyen, High-order micromechanical electronic filters, *Proceedings of the 10th Annual IEEE International Workshop on Micro Electro Mechanical Systems*, Nagoya, 1997, pp. 25–30.
[14] D. Weinstein, S.A. Bhave, M. Tada, S. Mitarai, S. Morita, K. Ikeda, Mechanical coupling of 2D resonator arrays for MEMS filter applications, *Proceedings of the 2007 IEEE International Frequency Control Symposium*, Geneva, 2007, pp. 1362–1365.
[15] L. Meirovitch, *Elements of Vibration Analysis*, McGraw-Hill, New York, 1986.
[16] B.J. Olson, Order-tuned vibration absorbers for systems with cyclic symmetry with applications to turbomachinery, Michigan State University, East Lansing, 2006.
[17] M. Shavezipur, K. Ponnambalam, A. Khajepour, S.M. Hashemi, Fabrication uncertainties and yield optimization in MEMS tunable capacitors, *Sensors and Actuators A* 147 (2008) 613–622.
[18] M.A. Abdelmoneum, M.U. Demirci, Y.W. Lin, C.T.-C. Nguyen, Post-fabrication laser trimming of micromechanical filters, *Proceedings of the 2004 IEEE International Electron Devices Meeting*, San Francisco, 2004, pp. 39–42.
[19] G.M. Rebeiz, *RF MEMS: Theory, Design and Technology*, John Wiley & Sons, Hoboken, 2003.
[20] Y. He, J. Marchetti, C. Gallegos, F. Maseeh, Accurate fully-coupled natural frequency shift of MEMS actuators due to voltage bias and other external forces, *Proceedings of the 12th IEEE International Conference on Micro Electro Mechanical Systems*, Orlando, 1999, pp. 17–21.
[21] T. Remtema, L. Lin, Active frequency tuning for micro resonators by localized thermal stressing effects, *Sensors and Actuators A* 91 (2001) 326–332.
[22] A. Dubi, *Monte Carlo Applications in Systems Engineering*, John Wiley & Sons, New York, 1999.
[23] V.B. Chivukula, *MEMS Bandpass Filters Based on Cyclic Coupling Architectures*, Purdue University, West Lafayette, 2009.